

SeaCache: Spectral-Evolution-Aware Cache for Accelerating Diffusion Models

Jiwoo Chung^{1,†} Sangeek Hyun¹ MinKyu Lee¹ Byeongju Han²
 Geonho Cha² Dongyoon Wee² Youngjun Hong^{2,*} Jae-Pil Heo^{1,*}

¹Sungkyunkwan University ²NAVER Cloud

Abstract

Diffusion models are a strong backbone for visual generation, but their inherently sequential denoising process leads to slow inference. Previous methods accelerate sampling by caching and reusing intermediate outputs based on feature distances between adjacent timesteps. However, existing caching strategies typically rely on raw feature differences that entangle content and noise. This design overlooks spectral evolution, where low-frequency structure appears early and high-frequency detail is refined later. We introduce Spectral-Evolution-Aware Cache (SeaCache), a training-free cache schedule that bases reuse decisions on a spectrally aligned representation. Through theoretical and empirical analysis, we derive a Spectral-Evolution-Aware (SEA) filter that preserves content-relevant components while suppressing noise. Employing SEA-filtered input features to estimate redundancy leads to dynamic schedules that adapt to content while respecting the spectral priors underlying the diffusion model. Extensive experiments on diverse visual generative models and the baselines show that SeaCache achieves state-of-the-art latency-quality trade-offs. Codes are available at github.com/jiwoogit/SeaCache.

1. Introduction

Recent diffusion [14, 48, 56–58] and rectified-flow (RF) [16, 38] models produce high-quality images and videos through iterative denoising. Despite this progress, sampling still requires tens to hundreds of steps, which turns user-facing applications into latency bound. A common remedy is to reduce the step count or the per-step cost through distillation [15, 26, 45, 50–52], quantization [8, 54, 70, 76], or efficient attention [67, 68, 71, 74, 75]. These approaches are effective but introduce added training overhead and dependence on task or data-specific tuning.

[†] This work was done during an internship at NAVER Cloud.

^{*} Co-corresponding authors.

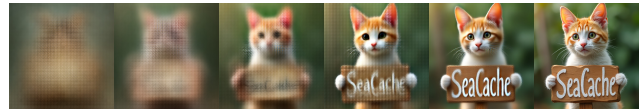
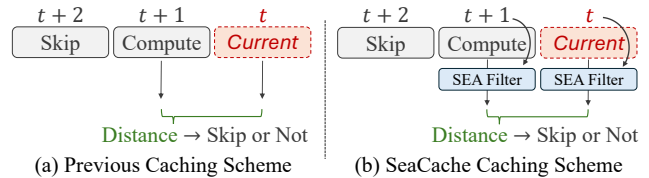


Figure 1. Conceptual illustration and motivation of the proposed caching scheme (SeaCache) compared with previous caching schemes. The lower panel shows a denoising trajectory of a cat image where coarse low-frequency structure appears at early steps and fine high-frequency details emerge at later steps, illustrating the spectral evolution of iterative generative models. SeaCache applies a Spectral-Evolution-Aware (SEA) Filter to raw diffusion features so that the distance measure better captures timestep-aware spectral residuals between timesteps.

A complementary direction exploits redundancy between consecutive steps via caching. Caching reduces the number of forward passes by reusing intermediate features from previous timesteps. Early work adopts static schedules [31, 36, 79] that cache features at fixed intervals along the trajectory, which yields predictable speedups. More recent methods introduce dynamic schedules [1, 6, 33] that decide when to reuse based on the distance between current and cached features, thereby reducing the error introduced by caching. These approaches focus on where to cache, for example which layers or blocks, while the error itself is still measured in the raw feature space.

However, these approaches measure errors directly in the raw feature space and overlook *spectral evolution*, a key prior underlying the denoising process. Independent of caching, prior studies [17, 22, 30, 73] have provided clear evidence that diffusion models exhibit spectral evolution, where ujkearly timesteps establish low-frequency structure and later timesteps refine high-frequency detail, as also illustrated in the lower panel of Fig. 1. From this viewpoint, spectral evolution at a given timestep can be interpreted as a

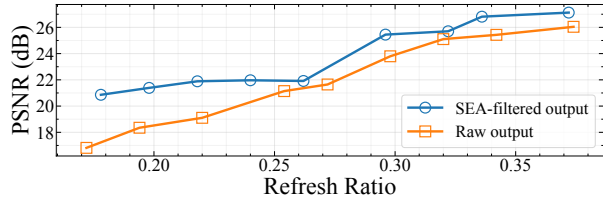
change in the signal-to-noise ratio. We use the term *signal* for the content-carrying component that is aligned with the clean sample and mainly lies in low frequencies, and *noise* for the residual component that is concentrated in high frequencies and reflects stochastic variation.

In this paper, we incorporate this spectral evolution, or equivalently the evolution of the signal-to-noise ratio, into cache scheduling. Rather than treating all spectral components equally, we design a cache metric that focuses on the signal component while downweighting the noise component. By grounding reuse decisions on discrepancies in the synthesized content, the resulting metric becomes less sensitive to high-frequency noise and encourages cache gating to respond to meaningful signal alignment rather than stochastic variation.

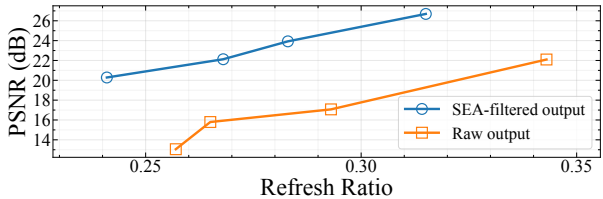
To validate this idea, we conduct an oracle experiment that compares cache schedules derived from raw feature distances with those derived from distances in a signal-emphasized space. In standard caching schemes, the decision to skip or compute is based on the distance between input features at consecutive timesteps. In our oracle analysis, we instead compare consecutive *output features*, thereby removing input-to-output approximation error and isolating the effect of spectral filtering. Specifically, we compare two criteria: one that measures distances after applying the SEA (Spectral-Evolution-Aware) filter, which downweights the noise component (Sec. 4.1), and another that uses unfiltered raw outputs, as shown in Fig. 2. The filtered criterion yields cache decisions that more closely track the full-compute trajectory, as evidenced by consistently higher PSNR. This suggests that spectrum-aware scheduling better preserves the behavior of the original model.

To this end, we propose Spectral-Evolution-Aware Cache (**SeaCache**), a simple yet effective caching scheme that encodes the spectral prior of iterative denoising models through a Spectral-Evolution-Aware (SEA) filter, as illustrated in Fig. 1. The SEA filter provides a practical scheduling policy by allowing cache decisions to be driven by the signal component. Before measuring feature distances, SeaCache passes intermediate features through a theoretically motivated, timestep-dependent filter that modulates the frequency response along the sampling trajectory. This operation acts as a lightweight reweighting that amplifies the content-relevant signal while downweighting noise-dominated components.

SeaCache is plug-and-play: it requires no architectural modification or retraining, and can be attached to existing caching policies by inserting a single filtering step before distance computation. The method is both network-agnostic and sampler-agnostic, enabling integration across diverse diffusion and rectified-flow models. In practice, SeaCache substantially reduces the number of forward passes while preserving the perceptual fidelity of the original outputs,



(a) Latency-quality trade-off on *FLUX*.



(b) Latency-quality trade-off on *Wan2.1 1.3B*.

Figure 2. **Latency-quality trade-off in oracle experiments.** We compare cache decisions based on raw output differences and SEA-filtered output differences (Sec. 4.1) on *FLUX* [28, 29] and *Wan2.1 1.3B* [63]. The refresh ratio is the fraction of timesteps that run a full denoiser evaluation instead of reusing cached features. For each criterion, PSNR is computed between the cached sample and the corresponding full timestep (no-cache) sample, averaged over each prompt set [23, 49]. At matched refresh ratios, the filtered criterion consistently achieves higher PSNR with respect to the full-compute trajectory, validating the effectiveness of a spectrum-aware distance for cache scheduling.

and it consistently improves the latency-quality trade-off over prior caching schemes across experiments.

Our main contributions are threefold.

- We propose **SeaCache**, a simple yet effective caching policy that bases reuse decisions on a timestep-aligned spectral representation of the generative trajectory.
- We revisit prior caching strategies and show that raw feature metrics ignore spectral evolution, while our formulation bases cache decisions on content rather than noise.
- Extensive experiments on multiple visual generative models show that our method achieves better latency-quality trade-offs than prior caching baselines.

2. Related Work

2.1. Generative Model Acceleration

Recent generative models [10, 14, 16, 38, 48, 56–58] have advanced visual synthesis, but their multi-step denoising procedures make inference latency and computation a primary bottleneck. Step reduction methods compress the sampling trajectory using improved solvers [39, 57, 78] and distillation-based samplers [40, 50, 59]. These approaches are effective but require additional training and often modify the original model. Another line of work reduces the cost of each step through quantization [20, 32, 54, 55], efficient attention [3, 12, 13, 47, 67, 68, 71, 74, 75], and to-

ken reduction [25, 55, 75]. These techniques lower FLOPs while preserving the sequential dependency of the sampler, but they typically demand extra resources and engineering effort. This limitation motivates caching-based acceleration, which exploits redundancy across successive timesteps to reuse intermediate features without additional training.

2.2. Caching-based Acceleration

Caching-based acceleration reuses intermediate computations across adjacent timesteps without retraining. Early methods [31, 42, 66] achieve speedups by reusing features but are designed for U-Net architectures, which limits their applicability to transformer-based models. To address this limitation, later work [9, 34, 53] adapts caching to DiT architectures [31, 53] for image synthesis. For video, PAB [79] selects different timestep intervals for each attention block and achieves speedups.

These methods rely on static schedules and cannot adapt to input diversity, so recent work adopts dynamic policies that respond to the generated signal [2, 24, 33, 37, 41, 43]. For example, AdaCache [24] accounts for motion complexity for accelerating video generation. TeaCache [33] and DiCache [6] estimate output changes from distances measured near the input features and assume that these distances provide a reliable redundancy signal between adjacent-timesteps. In our work, we measure redundancy in a timestep-aligned spectral space that emphasizes content-carrying components. Unlike prior dynamic caching, SeaCache explicitly models *spectral evolution* through a timestep-conditioned SEA filter motivated by a linear-denoiser view, and applies gain normalization to enable stable distance measurements across timesteps. As a result, SeaCache is the first caching policy that injects an explicit frequency prior into the reuse decision.

Recent studies [35, 37, 81] explore reusing features differently across frequency bands. In contrast, we focus on when to reuse rather than how to utilize cached features. Leveraging the spectral evolution prior where low-frequency structure emerges early while high-frequency details are refined later, we propose a simple cache policy that plugs easily into existing caching baselines.

3. Preliminary

3.1. Denoising Generative Models

Diffusion probabilistic models (DPMs) [21] and rectified flow (RF) models [38] generate samples by iteratively removing noise. Let X denote a clean image or video, and let an encoder map X to a latent x_0 . For images, we denote $x_0 \in \mathbb{R}^{H \times W \times C}$, and for videos $x_0 \in \mathbb{R}^{H \times W \times F \times C}$, where H , W , F , and C denote the height, width, number of frames, and channels of the latent representation, respectively.

We adopt the standard forward noising model at discrete

solver steps $t \in \{0, \dots, T\}$:

$$x_t = a_t x_0 + b_t \varepsilon, \quad \varepsilon \sim \mathcal{N}(0, \mathbf{I}), \quad (1)$$

where T is the total number of steps and (a_t, b_t) are determined by the noise schedule. For DPMs [21], $a_t = \sqrt{\bar{\alpha}_t}$ and $b_t = \sqrt{1 - \bar{\alpha}_t}$ with $\bar{\alpha}_t \in [0, 1]$ given by the schedule. For RFs [38], the same linear mixture provides a useful approximation with $a_t = 1 - \alpha_t$ and $b_t = \alpha_t$, where $\alpha_t = \frac{t}{T}$.

Under this noise mixture model, DPMs are trained to predict the noise ε from the noised latent x_t at timestep t . The corresponding training objective is

$$\mathcal{L}_{\text{DPM}} = \mathbb{E}_{x_0, t, \varepsilon, y} [\|\varepsilon - \epsilon_\theta(x_t, t, y)\|_2^2], \quad (2)$$

where y is a conditioning signal and ϵ_θ is a denoising network that estimates the noise added to x_0 . Sampling proceeds in reverse, starting from $x_T \approx \varepsilon$ and iteratively reconstructing x_0 . This iterative denoising process induces strong redundancy between outputs at adjacent timesteps, and cache-based acceleration exploits this redundancy by reusing intermediate predictions.

3.2. Timestep-Aware Dynamic Caching

A recent approach, TeaCache [33], quantifies change at step t using the timestep-modulated input $I_t = \phi(x_t, t)$, where ϕ injects a timestep embedding into the input x_t . This proxy is strongly correlated with the denoiser output O_t while remaining inexpensive to compute, and for brevity we refer to I_t as the input feature. The relative ℓ_1 distance is then defined as

$$\Delta_t = \text{L1}_{\text{rel}}(I_t, I_{t+1}) = \frac{\|I_t - I_{t+1}\|_1}{\|I_{t+1}\|_1 + \xi}, \quad (3)$$

with a small constant ξ for numerical stability [6, 33, 42].

After computing the model output at step t_a , the same output is reused for steps $t \in [t_a, t_b - 1]$ until the accumulated change exceeds a threshold δ . Let $t_b > t_a$ be the smallest index that satisfies

$$\sum_{s=t_a}^{t_b-1} \Delta_s \leq \delta < \sum_{s=t_a}^{t_b} \Delta_s, \quad (4)$$

at which point a refresh is triggered at t_b and the accumulator is reset. Smaller δ leads to more frequent refreshes and higher fidelity, while larger δ increases speed at the risk of artifacts. We follow the accumulated-distance rule and keep the same refresh logic on the timestep-modulated feature at the pre-attention input of the first transformer block to maximize skipped computation, as in TeaCache. Accordingly, SeaCache injects spectral priors into Δ_t by measuring change in a frequency-aware filtered representation.

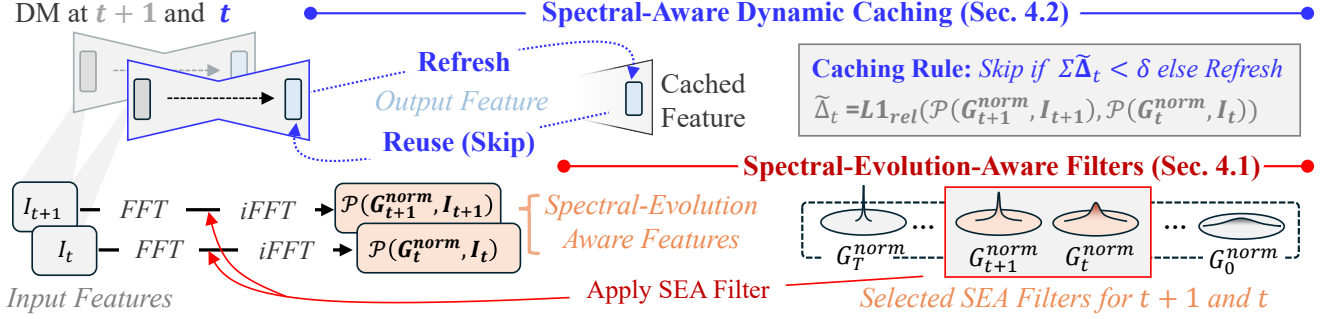


Figure 3. **Overview of SeaCache.** Given input features I_t and I_{t+1} , SeaCache first applies FFT, multiplies by the timestep-dependent SEA filters G_t^{norm} and G_{t+1}^{norm} , and then applies iFFT to obtain spectral-evolution-aware features $\mathcal{P}(G_t^{\text{norm}}, I_t)$ and $\mathcal{P}(G_{t+1}^{\text{norm}}, I_{t+1})$ (Sec. 4.1). A spectrum-aware dynamic caching module (Sec. 4.2) measures the relative distance $\tilde{\Delta}_t$ between consecutive filtered features, accumulates it over timesteps, and either reuses the cached output or refreshes the denoiser when the threshold δ is exceeded. The underlying diffusion model remains unchanged, so SeaCache acts as a plug-and-play cache policy that replaces only the distance metric.

4. Method: SeaCache

Prior analyses [3, 22, 30] and the lower panel of Fig. 1 reveal a form of spectral evolution in diffusion models, where early steps build low-frequency structure and later steps refine high-frequency detail. Motivated by this behavior, we design a spectrum-aware reuse metric that guides cache scheduling across timesteps. Our approach proceeds in three stages (Fig. 3). First, in Sec. 4.1, we formalize the denoiser frequency response and derive a timestep-dependent filter that captures this evolution. Second, in Sec. 4.2, we introduce an input proxy whose filtered distance is closely related to the filtered output distance, which enables a training-free, plug-and-play schedule. Finally, we replace the original metric Δ_t with its spectrum-aware counterpart $\tilde{\Delta}_t$ while preserving the standard accumulated distance based refresh rule.

4.1. Spectral-Evolution-Aware Filter

To design a filter that reflects spectral evolution, we formalize how the effective frequency band changes across timesteps. Motivated by Spectral Diffusion [72], we adopt the timestep-dependent frequency response derived under the optimal linear denoiser. For notational simplicity, we describe a single-channel 2D filter. In implementation, the filter is applied per-channel over the spatial (2D) axes for images and over the spatiotemporal (3D) axes for videos.

We consider the linear minimum mean squared error (MMSE) estimator $\hat{x}_0 = h_t * x_t$ obtained by minimizing $J_t(h_t) = \|h_t * x_t - x_0\|_2^2$, where h_t is a linear denoising filter and $*$ denotes convolution (which corresponds to pointwise multiplication in the frequency domain). We denote by h_t^* the optimal linear filter that minimizes J_t . Let $G_t(f)$ denote the frequency response of the optimal linear denoising filter h_t^* at frequency f , and let $S_x(f)$ denote the power spectrum of x_0 at frequency f . Under the linear mixture in Eq. 1, the optimal frequency response of h_t^* takes a

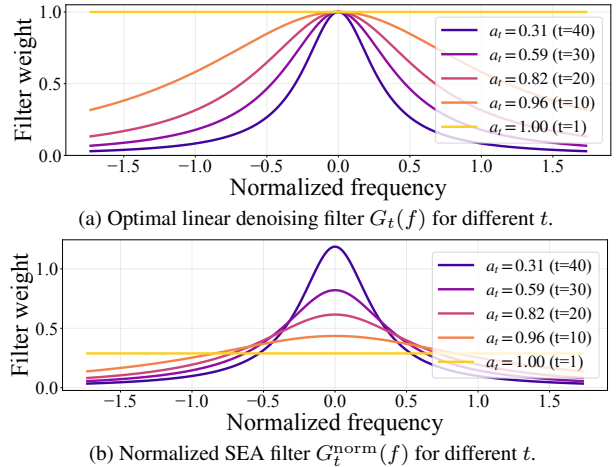


Figure 4. **Visualization of timestep-dependent denoising filters.** (a) Optimal linear denoising responses $G_t(f)$ across timesteps, where early steps primarily pass low-frequencies and later steps gradually include higher frequencies, reflecting spectral evolution. (b) Corresponding normalized filters $G_t^{\text{norm}}(f)$ with unit mean gain, which stabilize filtered feature energy across timesteps and are used as SEA filters for cache scheduling.

Wiener-like form [65]:

$$G_t(f) = \frac{a_t S_x(f)}{a_t^2 S_x(f) + b_t^2}, \quad (5)$$

and although the linearity assumption on h_t is restrictive, it still provides useful insight into spectral evolution.

Assuming a natural power law spectrum [7, 18, 61, 62] for $S_x(f)$, representative DPM responses $G_t(f)$ are shown in Fig. 4a. In the reverse diffusion process, t decreases from T to 0 while a_t increases from 0 to 1, gradually recovering high frequency detail in a way that is consistent with spectral evolution. The resulting filters for DPMs and RF models exhibit nearly identical behavior, and for brevity we present the analysis in terms of the DPM in the main text.

Full derivations are provided in the supplementary material. In this view, we refer to the low-frequency content-carrying component aligned with the clean sample as the signal and to the high-frequency residual that primarily reflects stochastic variation as noise.

We formulate the optimal response $G_t(f)$ and confirm spectral evolution under this model. We then use $G_t(f)$ to filter features in the frequency domain for constructing a spectrum-aware representation that emphasizes the signal component while suppressing noise. Specifically, we define a feature-level mapping \mathcal{P}_t by applying the fast Fourier transform (FFT [46]), multiplying by the timestep-dependent spectrum-aware filter $G_t(f)$, and returning to the original space via the inverse FFT (iFFT):

$$\mathcal{P}(G_t, I_t) = \text{iFFT}(G_t(f) \odot \text{FFT}(I_t)), \quad (6)$$

where f indexes radial frequencies on the discrete Fourier grid and \odot denotes element-wise multiplication with broadcasting across channels and spatial or spatiotemporal dimensions. This operator $\mathcal{P}_t(G_t, \cdot)$ induces a timestep-dependent passband and defines the filtered feature space in which spectrum-aware cache distances are computed.

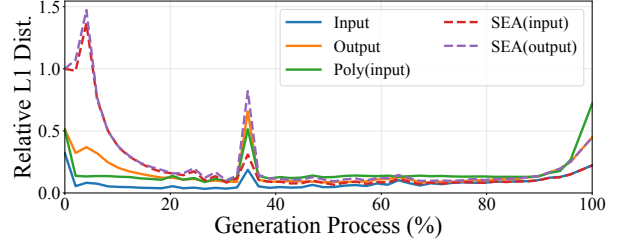
Before filtering the features, the raw response G_t exhibits a timestep-dependent gain, as in the varying radial averages in Fig. 4a. To ensure that distances are comparable across timesteps, we normalize this gain by enforcing a constant mean over radial frequencies, yielding density-normalized response G_t^{norm} (Fig. 4b). Specifically, let the discrete radial frequencies on the FFT grid be $\mathcal{F} = \{f_\ell\}_{\ell=0}^{L-1}$, where L is the number of radial bins, induced by the spatial resolution $H \times W$ for images. We define

$$\nu_t = \left(\frac{1}{L} \sum_{f_\ell \in \mathcal{F}} G_t(f_\ell) \right)^{-1}, \quad G_t^{\text{norm}}(f) = \nu_t G_t(f), \quad (7)$$

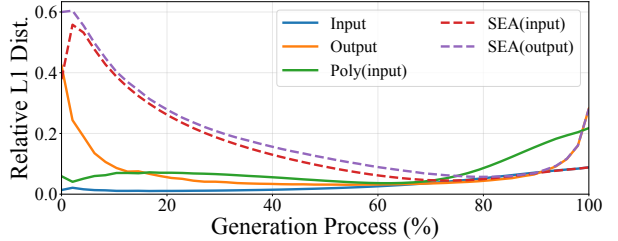
where ν_t is average energy over radial bins such that G_t^{norm} has constant mean gain over \mathcal{F} . Using this density normalized filter, we empirically observe that distances computed after filtering better reflect denoising redundancy than their raw counterparts, and we use G_t^{norm} for our SEA filter in the subsequent caching schedule.

4.2. Spectrum-Aware Dynamic Caching

Prior caching methods [6, 34, 36, 42, 66] typically assume that differences between consecutive model outputs reflect redundancy relative to a full-compute trajectory. Building on this assumption, they construct dynamic schedules by approximating output differences from input-side features such as intermediate layers or blocks. However, the oracle study in Sec. 1 and Fig. 2 show that this raw feature formulation is suboptimal. Cache decisions based on SEA-filtered outputs stay closer to the full compute trajectory than those based on raw outputs at the same refresh ratio.



(a) Relative ℓ_1 across the generation process on *FLUX*.



(b) Relative ℓ_1 across the generation process on *Wan2.1 1.3B*.

Figure 5. **Relative ℓ_1 across the generation process.** Stepwise relative ℓ_1 distances between consecutive timesteps for different feature choices, averaged over ten samples for each model. *Input* denotes distances on the timestep-modulated input features I_t . *Output* is the last block outputs O_t . *SEA(Input)*, *SEA(Output)* applies the SEA filter to the input and output features, respectively. *Poly(Input)* corresponds to the polynomial-fitted input distance which is designed to approximate output differences from input features. SEA-filtered inputs closely track SEA-filtered outputs across timesteps, whereas other inputs show weaker alignment.

Directly using SEA-filtered outputs in the cache metric is not practical, since the output O_t is only available after a full denoiser run and thus offers no speedup. We therefore seek an input-side proxy that matches the SEA-filtered output distance as closely as possible. Building on the input features I_t , introduced in Sec. 3.2, we compare several candidates: raw input I_t , raw output O_t , the polynomial fitted input used in TeaCache [33], and their SEA-filtered counterparts obtained by applying $\mathcal{P}_t(G_t, \cdot)$ from Sec. 4.1.

Fig. 5 reports the relative ℓ_1 distance between consecutive timesteps for these feature choices, averaged over ten samples on *FLUX* and *Wan2.1 1.3B*. The SEA-filtered input distances $\mathcal{P}_t(G_t, I_t)$ closely follow the SEA-filtered output distances $\mathcal{P}_t(G_t, O_t)$ along the entire trajectory, while raw input and polynomial fitted input show weaker alignment, especially at early timesteps. Moreover, the SEA-filtered input distances are larger at early timesteps, which is consistent with the common practice of always recomputing early steps in many prior caching schemes [6, 36, 42, 43]. This empirical finding is desirable because the SEA filter suppresses stochastic noise while preserving content-carrying components, which makes adjacent-timestep features more stable and faithful proxies for output change. These results support SEA-filtered inputs as a reliable, training-free proxy for adapting spectrum-aware redundancy.

Table 1. Quantitative comparison in *FLUX.1-dev* [28, 29].

Method	Latency (s)	TFLOPs	PSNR \uparrow	LPIPS \downarrow	SSIM \uparrow
Original (50 steps)	20.9	2976	–	–	–
Vanilla 25 steps	10.5	1487	15.553	0.409	0.668
Vanilla 15 steps	6.4	892	17.842	0.305	0.740
TeaCache ($\delta=0.3$)	11.4	1547	20.762	0.211	0.810
TaylorSeer ($\mathcal{S}=3$)	9.8	1191	22.783	0.163	0.828
SeaCache ($\delta=0.3$)	9.4	1098	26.285	0.106	0.893
Δ -Dit	15.5	1984	17.403	0.336	0.710
ToCa	15.9	1263	18.398	0.324	0.700
TeaCache ($\delta=0.6$)	7.1	892	17.214	0.348	0.714
TaylorSeer ($\mathcal{S}=5$)	7.5	834	19.972	0.236	0.762
SeaCache ($\delta=0.6$)	6.4	773	21.332	0.226	0.798

Table 2. Comparison of average rank on CycleReward [4].

Method ($\approx 50\%$)	Rank \downarrow	Method ($\approx 30\%$)	Rank \downarrow
TeaCache ($\delta=0.3$) [33]	2.01	TeaCache ($\delta=0.6$) [33]	2.07
TaylorSeer ($\mathcal{S}=3$) [36]	2.08	TaylorSeer ($\mathcal{S}=5$) [36]	1.98
SeaCache ($\delta=0.3$)	1.91	SeaCache ($\delta=0.6$)	1.96

In SeaCache, distance is therefore measured after density normalized filtering, and the per-step cache metric is defined as

$$\tilde{\Delta}_t = \text{L1}_{\text{rel}}(\mathcal{P}(G_t^{\text{norm}}, I_t), \mathcal{P}(G_{t+1}^{\text{norm}}, I_{t+1})). \quad (8)$$

The accumulated distance rule in Eq. (4) is kept unchanged. After a refresh at t_a , the cached output is reused for $t \in [t_a, t_b - 1]$, and the next refresh occurs at the smallest t_b whose accumulated distance exceeds the threshold δ . This yields a spectral-evolution-aware, timestep-dependent gate that is training-free and architecture-agnostic, and depends only on the shared sampler schedule coefficients (a_t, b_t) .

5. Experiments

5.1. Experimental Settings

Model configurations. We evaluate on three state-of-the-art visual generative models. FLUX.1-dev [28, 29] is a text-to-image model. HunyuanVideo [27] and Wan2.1 [63] are text-to-video models. For Wan2.1, we use the 1.3B pre-trained checkpoint. All models are sampled for 50 steps under their default configurations. For example, when using TaylorSeer [36], we follow its default settings and set the expansion order to 1 for FLUX.1-dev and to 2 for HunyuanVideo and Wan2.1. FLUX experiments run on NVIDIA Blackwell Pro 6000 GPUs, and HunyuanVideo and Wan2.1 are evaluated on NVIDIA A100 GPUs.

Baseline configurations. TeaCache [33] is applied using the official implementation with default settings, and we adjust the distance threshold δ to control the cache ratio. TaylorSeer [36] is also used with the official code. For a fair comparison, we explicitly refresh the first five timesteps for images and the first three timesteps for videos, and we adjust the stride \mathcal{S} to control the cache ratio. ToCa [80] and

Table 3. Quantitative comparison in *HunyuanVideo* [27].

Method	Latency (s)	TFLOPs	PSNR \uparrow	LPIPS \downarrow	SSIM \uparrow
Original (50 steps)	182.6	14038	–	–	–
Vanilla 25 steps	93.7	7019	19.97	0.263	0.731
Vanilla 15 steps	56.8	4211	17.49	0.371	0.662
TeaCache ($\delta=0.12$)	98.5	6994	23.40	0.133	0.805
TaylorSeer ($\mathcal{S}=2$)	96.9	7299	24.14	0.152	0.820
SeaCache ($\delta=0.19$)	90.8	6747	32.39	0.047	0.932
TeaCache ($\delta=0.2$)	64.4	4794	20.42	0.172	0.734
TaylorSeer ($\mathcal{S}=3$)	68.8	5053	20.42	0.242	0.733
SeaCache ($\delta=0.35$)	58.1	4598	26.46	0.133	0.857

DiCache [6] are employed through their official implementations under default settings. For Δ -DiT [9], we follow the reference implementation provided with TaylorSeer.

Evaluation protocol. For all experiments, generated images and videos are stored as PNG and MP4 files, respectively. For text-to-image generation, we evaluate 200 DrawBench prompts [49] and generate 1024×1024 images. For text-to-video generation, we use 944 prompts from VBench [23] and generate a 480p video with 65 frames per prompt. For each configuration, the full timestep output of the original model serves as the reference, and PSNR (computed on RGB values), LPIPS [77], and SSIM [64] are computed between each cached sample and its reference and then averaged over all samples. TFLOPs are measured with Calflops [69] and reported in tera operations. We further assess perceptual quality using CycleReward [4], a state-of-the-art image reward benchmark. The initial random seed is shared across our method and all baselines, and we consider two cache budgets, approximately 50% and 30%.

5.2. Quantitative Comparison

Text-to-image generation. We compare SeaCache with existing caching methods on *FLUX.1-dev* [28, 29] in Tab. 1. At a moderate budget (roughly 50% refresh ratio), TeaCache [33] and TaylorSeer [36] stay close to the 25 step baseline, while SeaCache further reduces latency and FLOPs and at the same time improves PSNR, LPIPS, and SSIM. This trend persists under stronger acceleration (roughly 30% refresh ratio). Baselines exhibit clear drops in reconstruction quality, whereas SeaCache achieves the fastest setting among caching methods and still attains the best metrics, yielding a stronger latency-quality trade-off.

We also assess perceptual quality using CycleReward [4] in Tab. 2. At both budgets ($\approx 50\%$ and $\approx 30\%$), SeaCache achieves the lowest average reward rank among TeaCache and TaylorSeer, showing a better latency-quality trade-off for both reconstruction fidelity and preference.

Text-to-video generation. For *HunyuanVideo* [27], in Tab. 3, SeaCache consistently achieves a stronger latency-quality trade-off than the baselines. In the higher cache budget setting (upper block), SeaCache reduces latency and



Figure 6. Qualitative comparison of SeaCache and baselines on *FLUX* at refresh ratios of approximately 30% and 50%.

Table 4. Quantitative comparison in *Wan2.1 1.3B* [63].

Method	Latency (s)	TFLOPs	PSNR \uparrow	LPIPS \downarrow	SSIM \uparrow
Original (50 steps)	176.3	8214	–	–	–
TeaCache ($\delta=0.09$)	86.6	4107	20.84	0.171	0.721
TaylorSeer ($S=2$)	93.1	4189	16.15	0.336	0.543
SeaCache ($\delta=0.2$)	83.9	3942	26.60	0.075	0.873
TeaCache ($\delta=0.15$)	63.6	2957	18.88	0.245	0.645
TaylorSeer ($S=3$)	67.1	2956	14.18	0.455	0.453
SeaCache ($\delta=0.35$)	56.6	2793	21.78	0.170	0.740

TFLOPs while improving all metrics. PSNR increases by roughly 8 dB over the strongest baseline, with lower LPIPS and higher SSIM. In the more aggressive setting (lower block), this trend remains. SeaCache runs faster than the baselines and still delivers clearly better overall metrics, whereas other methods show noticeable degradation.

For *Wan2.1 1.3B* [63], a similar pattern appears in Tab. 4. At the higher cache budget (upper block), SeaCache again reduces latency and TFLOPs while providing substantially higher PSNR and SSIM and lower LPIPS than TeaCache and TaylorSeer. Under the aggressive setting (lower block), SeaCache also shows the fastest latency and preserves reconstruction quality effectively, with consistently better metrics. Overall, these results indicate that the spectrum-aware schedule of SeaCache transfers well to video models and validate superior performance across architectures.

5.3. Qualitative Comparison

Text-to-image generation. In Fig. 6, we compare SeaCache with TeaCache [33] and TaylorSeer [36] at two cache budgets with refresh ratios of approximately 30% and 50%. SeaCache preserves both the semantic content and overall perceptual quality of the original images, whereas the baselines frequently lose text or fine details. At a 30% refresh ratio, the baselines fail to reproduce the word “quantum” specified in the prompt, while SeaCache faithfully preserves the text present in the fully computed image. At a 50% refresh ratio (second row), SeaCache generates two orange plates consistent with both the prompt and the original im-

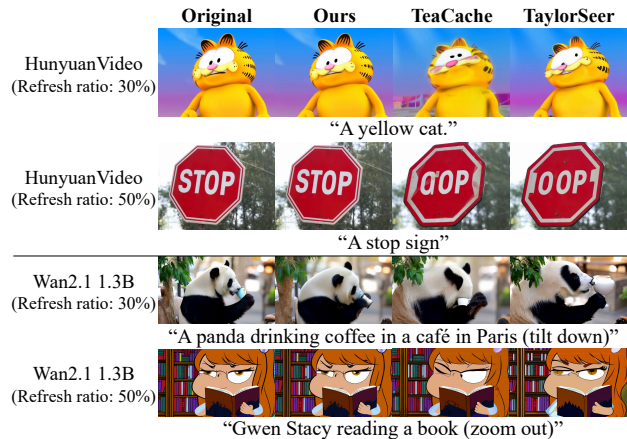


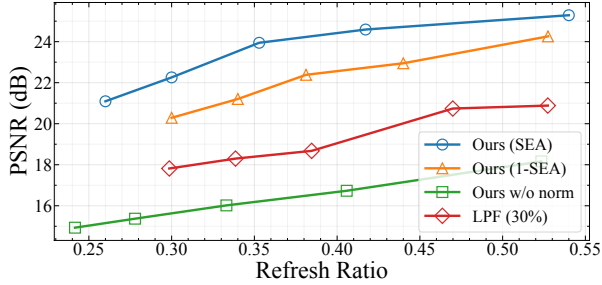
Figure 7. Qualitative comparison of text-to-video generative models at refresh ratios of approximately 30% and 50%.

age, whereas the baselines either alter the plate color by filling the plates with food or remove one of the plates.

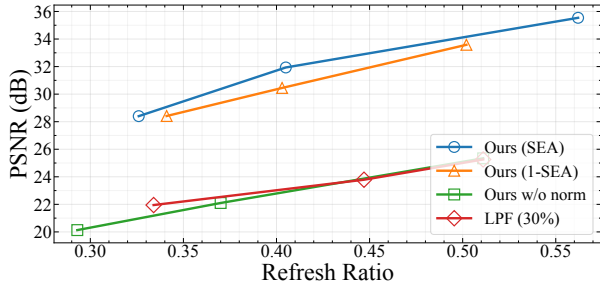
Text-to-video generation. We further conduct qualitative comparisons on text-to-video models *HunyuanVideo* and *Wan2.1 1.3B*, as shown in Fig. 7. For each prompt, we display the same frame index for the original model. Our cache scheme preserves the content of the original implementation while using a comparable computation budget. In the second row of *HunyuanVideo*, SeaCache maintains a sharp and legible “STOP” sign that closely matches the original, whereas the baselines fail to synthesize the letters. In the third row on *Wan2.1 1.3B*, SeaCache produces clear pandas and coffee cups with fewer artifacts, while competing methods blur the foreground and introduce the distortions.

5.4. Additional Analysis

Ablation study. We quantitatively evaluate the effect of each design choice in SeaCache. Fig. 8 compares four variants of the cache distance: the SEA filter, its complementary form 1–SEA, a version without normalization, and a simple cutoff low-pass filter that only keeps the component of lowest 30% frequency. Across both *FLUX* and *Hunyuan-*



(a) PSNR-refresh ratio trade-off on *FLUX* [28, 29].



(b) PSNR-refresh ratio trade-off on *HunyuanVideo* [27].

Figure 8. **Ablation on spectrum-aware filtering.** Trade-offs for different cache metrics on *FLUX* and *HunyuanVideo*. Results are averaged over 200 prompts for *FLUX* and 20 randomly selected from VBench for *HunyuanVideo*, with the other settings fixed.

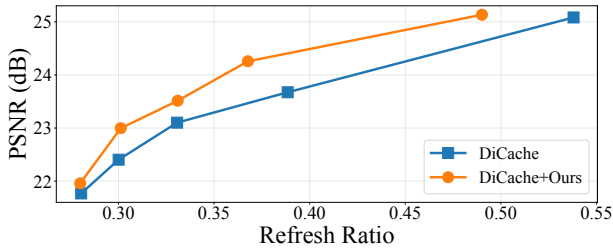


Figure 9. **Plug-and-play adaptation to DiCache.** PSNR-refresh ratio trade-off on *FLUX* when applying the SEA-based cache metric to DiCache [6]. “DiCache+Ours” denotes DiCache combined with our SEA filter, while “DiCache” uses the original metric.

Video, the SEA filter shows the best PSNR-refresh ratio trade-off, while 1-SEA produces a similar but consistently lower curve, indicating that tracking the spectral evolution of the noise component is somewhat informative but less aligned with content redundancy than our signal-focused design. Removing normalization leads to a drop in PSNR, since the filtered feature magnitude drifts across timesteps and the cache metric becomes biased. The static low-pass baseline (LPF 30%) also performs noticeably worse than ours with SEA filter, showing that simply emphasizing low frequencies is insufficient and that the timestep-dependent spectral evolution captured by the SEA filter is crucial for effective cache scheduling.

Adaptation to other cache methods. To examine the plug-and-play nature of SeaCache, we integrate the SEA filter

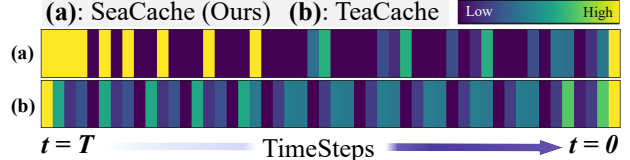


Figure 10. **Refresh pattern across timesteps on *FLUX*.** Per-timestep refresh ratio at a 30% budget. (a) SeaCache automatically concentrates refreshes on early timesteps, whereas (b) TeaCache spreads refreshes more uniformly over the trajectory.

into DiCache [6], a recent dynamic caching method that bases its metric on intermediate blocks. Instead of modifying the policy or network, we apply our SEA filtering to DiCache’s block-level features and reuse its original accumulation rule. On *FLUX*, the adapted variant (DiCache+Ours) achieves consistently higher PSNR for the same refresh ratio than the original DiCache, as shown in Fig. 9, while keeping latency and FLOPs comparable. This result indicates that the proposed spectrum-aware distance is not limited to input-side features and can also enhance cache metrics defined on intermediate representations, suggesting broad compatibility with future caching schemes.

Cache ratio visualization. For each timestep in *FLUX* with the 30% refresh ratio setting, Fig. 10 shows the fraction of samples that trigger a refresh among 200 Draw-Bench prompts. Bright cells indicate steps that are frequently computed, while dark cells correspond to steps that are almost always skipped. Many prior open-source methods [6, 36, 42] fix several early steps to always compute in order to improve quality, introducing an extra hyperparameter that should be tuned by hand. SeaCache instead concentrates most refreshes on early timesteps, aligned with the spectral-evolution prior, whereas TeaCache [33] distributes refreshes in a more gridlike pattern that does not adapt to timestep importance in Fig. 10. This adaptive schedule removes the need to manually choose how many early steps to compute and uses the cache budget more effectively.

6. Conclusion

We study cache-based acceleration for diffusion models via spectral evolution, showing that raw feature distances used in prior cache-based approaches fail to separate the signal and the noise. We introduce SeaCache, a training-free policy that bases reuse decisions on a spectrally aligned space. From this analysis, we derived the Spectral-Evolution-Aware (SEA) filter, whose distances follow the full-compute trajectory more faithfully than unfiltered metrics. By applying the SEA filter to input features, we obtain the schedules that adapt to content while respecting the spectral priors of the underlying diffusion model. We expect that incorporating spectral evolution into cache design can be combined with future acceleration methods.

Acknowledgments

This work was partly supported by NAVER Cloud Corporation, MSIT/IITP (No. RS-2022-II220680, RS-2020-II201821, RS-2019-II190421, RS-2024-00459618, RS-2024-00360227, RS-2024-00437633, RS-2024-00437102, RS-2025-25442569), MSIT/NRF (No. RS-2024-00357729), and KNPA/KIPoT (No. RS-2025-25393280)

References

- [1] Muhammad Adnan, Nithesh Kurella, Akhil Arunkumar, and Prashant J Nair. Foresight: Adaptive layer reuse for accelerated and high-quality text-to-video generation. *arXiv preprint arXiv:2506.00329*, 2025. 1
- [2] Anirud Aggarwal, Abhinav Shrivastava, and Matthew Gwilliam. Evolutionary caching to accelerate your off-the-shelf diffusion model. *arXiv preprint arXiv:2506.15682*, 2025. 3
- [3] Sotiris Anagnostidis, Gregor Bachmann, Yeongmin Kim, Jonas Kohler, Markos Georgopoulos, Artsiom Sanakoyeu, Yuming Du, Albert Pumarola, Ali Thabet, and Edgar Schönfeld. Flexidit: Your diffusion transformer can easily generate high-quality samples with less compute. In *Proceedings of the Computer Vision and Pattern Recognition Conference*, pages 28316–28326, 2025. 2, 4
- [4] Hyojin Bahng, Caroline Chan, Fredo Durand, and Phillip Isola. Cycle consistency as reward: Learning image-text alignment without human preferences. 2025. 6
- [5] David H Brandwood. A complex gradient operator and its application in adaptive array theory. In *IEE Proceedings F (Communications, Radar and Signal Processing)*, pages 11–16. IET, 1983. 1
- [6] Jiazi Bu, Pengyang Ling, Yujie Zhou, Yibin Wang, Yuhang Zang, Dahua Lin, and Jiaqi Wang. Docache: Let diffusion model determine its own cache. *arXiv preprint arXiv:2508.17356*, 2025. 1, 3, 5, 6, 8
- [7] Geoffrey J Burton and Ian R Moorhead. Color and spatial structure in natural scenes. *Applied optics*, 26(1):157–170, 1987. 4, 2
- [8] Lei Chen, Yuan Meng, Chen Tang, Xinzhu Ma, Jingyan Jiang, Xin Wang, Zhi Wang, and Wenwu Zhu. Q-dit: Accurate post-training quantization for diffusion transformers. In *Proceedings of the Computer Vision and Pattern Recognition Conference*, pages 28306–28315, 2025. 1
- [9] Pengtao Chen, Mingzhu Shen, Peng Ye, Jianjian Cao, Chongjun Tu, Christos-Savvas Bouganis, Yiren Zhao, and Tao Chen. Δ -DiT: A training-free acceleration method tailored for diffusion transformers. *arXiv preprint arXiv:2406.01125*, 2024. 3, 6
- [10] Jiwoo Chung, Sangeek Hyun, Hyunjun Kim, Eunseo Koh, MinKyu Lee, and Jae-Pil Heo. Fine-tuning visual autoregressive models for subject-driven generation. *arXiv preprint arXiv:2504.02612*, 2025. 2
- [11] LightX2V Contributors. Lightx2v: Light video generation inference framework. <https://github.com/ModelTC/lightx2v>, 2025. 2, 4
- [12] Tri Dao. FlashAttention-2: Faster attention with better parallelism and work partitioning. In *International Conference on Learning Representations (ICLR)*, 2024. 2
- [13] Tri Dao, Daniel Y. Fu, Stefano Ermon, Atri Rudra, and Christopher Ré. FlashAttention: Fast and memory-efficient exact attention with IO-awareness. In *Advances in Neural Information Processing Systems (NeurIPS)*, 2022. 2
- [14] Prafulla Dhariwal and Alexander Nichol. Diffusion models beat gans on image synthesis. *Advances in neural information processing systems*, 34:8780–8794, 2021. 1, 2
- [15] Hangliang Ding, Dacheng Li, Runlong Su, Peiyuan Zhang, Zhijie Deng, Ion Stoica, and Hao Zhang. Efficient-vdit: Efficient video diffusion transformers with attention tile. *arXiv preprint arXiv:2502.06155*, 2025. 1
- [16] Patrick Esser, Sumith Kulal, Andreas Blattmann, Rahim Entezari, Jonas Müller, Harry Saini, Yam Levi, Dominik Lorenz, Axel Sauer, Frederic Boesel, et al. Scaling rectified flow transformers for high-resolution image synthesis. In *Forty-first international conference on machine learning*, 2024. 1, 2
- [17] Fabian Falck, Teodora Pandevara, Kiarash Zahirnia, Rachel Lawrence, Richard Turner, Edward Meeds, Javier Zazo, and Sushrut Karmalkar. A fourier space perspective on diffusion models. *arXiv preprint arXiv:2505.11278*, 2025. 1
- [18] David J Field. Relations between the statistics of natural images and the response properties of cortical cells. *Journal of the Optical Society of America A*, 4(12):2379–2394, 1987. 4, 2
- [19] Xiaoliu Guan, Lielin Jiang, Hanqi Chen, Xu Zhang, Jiaying Yan, Guanzhong Wang, Yi Liu, Zetao Zhang, and Yu Wu. Forecasting when to forecast: Accelerating diffusion models with confidence-gated taylor. *Knowledge-Based Systems*, page 114635, 2025. 2
- [20] Yefei He, Luping Liu, Jing Liu, Weijia Wu, Hong Zhou, and Bohan Zhuang. Ptqd: Accurate post-training quantization for diffusion models. *Advances in Neural Information Processing Systems*, 36:13237–13249, 2023. 2
- [21] Jonathan Ho, Ajay Jain, and Pieter Abbeel. Denoising diffusion probabilistic models. *Advances in neural information processing systems*, 33:6840–6851, 2020. 3
- [22] Xingchang Huang, Corentin Salaun, Cristina Vasconcelos, Christian Theobalt, Cengiz Oztireli, and Gurprit Singh. Blue noise for diffusion models. In *ACM SIGGRAPH 2024 conference papers*, pages 1–11, 2024. 1, 4
- [23] Ziqi Huang, Yinan He, Jiashuo Yu, Fan Zhang, Chenyang Si, Yuming Jiang, Yuanhan Zhang, Tianxing Wu, Qingyang Jin, Nattapol Chanpaisit, et al. Vbench: Comprehensive benchmark suite for video generative models. In *Proceedings of the IEEE/CVF Conference on Computer Vision and Pattern Recognition*, pages 21807–21818, 2024. 2, 6, 4
- [24] Kumara Kahatapitiya, Haozhe Liu, Sen He, Ding Liu, Menglin Jia, Chenyang Zhang, Michael S Ryoo, and Tian Xie. Adaptive caching for faster video generation with diffusion transformers. In *Proceedings of the IEEE/CVF International Conference on Computer Vision*, pages 15240–15252, 2025. 3
- [25] Minchul Kim, Shangqian Gao, Yen-Chang Hsu, Yilin Shen, and Hongxia Jin. Token fusion: Bridging the gap between

- token pruning and token merging. In *Proceedings of the IEEE/CVF Winter Conference on Applications of Computer Vision*, pages 1383–1392, 2024. 3
- [26] Yeongmin Kim, Sotiris Anagnostidis, Yuming Du, Edgar Schönfeld, Jonas Kohler, Markos Georgopoulos, Albert Pumarola, Ali Thabet, and Artsiom Sanakoyeu. Autoregressive distillation of diffusion transformers. In *Proceedings of the Computer Vision and Pattern Recognition Conference*, pages 15745–15756, 2025. 1
- [27] Weijie Kong, Qi Tian, Zijian Zhang, Rox Min, Zuozhuo Dai, Jin Zhou, Jiangfeng Xiong, Xin Li, Bo Wu, Jianwei Zhang, et al. Hunyuanvideo: A systematic framework for large video generative models. *arXiv preprint arXiv:2412.03603*, 2024. 6, 8, 2
- [28] Black Forest Labs. Flux. <https://github.com/black-forest-labs/flux>, 2024. 2, 6, 8
- [29] Black Forest Labs, Stephen Batifol, Andreas Blattmann, Frederic Boesel, Saksham Consul, Cyril Diagne, Tim Dockhorn, Jack English, Zion English, Patrick Esser, Sumith Kullal, Kyle Lacey, Yam Levi, Cheng Li, Dominik Lorenz, Jonas Müller, Dustin Podell, Robin Rombach, Harry Saini, Axel Sauer, and Luke Smith. Flux.1 kontext: Flow matching for in-context image generation and editing in latent space, 2025. 2, 6, 8
- [30] Haeil Lee, Hansang Lee, Seoyeon Gye, and Junmo Kim. Beta sampling is all you need: Efficient image generation strategy for diffusion models using stepwise spectral analysis. In *2025 IEEE/CVF Winter Conference on Applications of Computer Vision (WACV)*, pages 4215–4224. IEEE, 2025. 1, 4
- [31] Senmao Li, Taihang Hu, Fahad Shahbaz Khan, Linxuan Li, Shiqi Yang, Yaxing Wang, Ming-Ming Cheng, and Jian Yang. Faster diffusion: Rethinking the role of unet encoder in diffusion models. *CoRR*, 2023. 1, 3
- [32] Yanjing Li, Sheng Xu, Xianbin Cao, Xiao Sun, and Baochang Zhang. Q-dm: An efficient low-bit quantized diffusion model. *Advances in neural information processing systems*, 36:76680–76691, 2023. 2
- [33] Feng Liu, Shiwei Zhang, Xiaofeng Wang, Yujie Wei, Haonan Qiu, Yuzhong Zhao, Yingya Zhang, Qixiang Ye, and Fang Wan. Timestep embedding tells: It’s time to cache for video diffusion model. In *Proceedings of the Computer Vision and Pattern Recognition Conference*, pages 7353–7363, 2025. 1, 3, 5, 6, 7, 8, 2
- [34] Haozhe Liu, Wentian Zhang, Jinheng Xie, Francesco Faccio, Mengmeng Xu, Tao Xiang, Mike Zheng Shou, Juan Manuel Perez-Rua, and Jürgen Schmidhuber. Faster diffusion via temporal attention decomposition. 2025. 3, 5
- [35] Jiacheng Liu, Peiliang Cai, Qinming Zhou, Yuqi Lin, Deyang Kong, Benhao Huang, Yupei Pan, Haowen Xu, Chang Zou, Junshu Tang, et al. Freqca: Accelerating diffusion models via frequency-aware caching. *arXiv preprint arXiv:2510.08669*, 2025. 3
- [36] Jiacheng Liu, Chang Zou, Yuanhuiyi Lyu, Junjie Chen, and Linfeng Zhang. From reusing to forecasting: Accelerating diffusion models with taylorseers. *arXiv preprint arXiv:2503.06923*, 2025. 1, 5, 6, 7, 8
- [37] Jiacheng Liu, Chang Zou, Yuanhuiyi Lyu, Fei Ren, Shaobo Wang, Kaixin Li, and Linfeng Zhang. Specca: Accelerating diffusion transformers with speculative feature caching. In *Proceedings of the 33rd ACM International Conference on Multimedia*, pages 10024–10033, 2025. 3
- [38] Xingchao Liu, Chengyue Gong, and Qiang Liu. Flow straight and fast: Learning to generate and transfer data with rectified flow. In *The Eleventh International Conference on Learning Representations (ICLR)*, 2023. 1, 2, 3
- [39] Cheng Lu, Yuhao Zhou, Fan Bao, Jianfei Chen, Chongxuan Li, and Jun Zhu. Dpm-solver: A fast ode solver for diffusion probabilistic model sampling in around 10 steps. *Advances in neural information processing systems*, 35:5775–5787, 2022. 2
- [40] Simian Luo, Yiqin Tan, Longbo Huang, Jian Li, and Hang Zhao. Latent consistency models: Synthesizing high-resolution images with few-step inference. *arXiv preprint arXiv:2310.04378*, 2023. 2
- [41] Zhengyao Lv, Chenyang Si, Junhao Song, Zhenyu Yang, Yu Qiao, Ziwei Liu, and Kwan-Yee K Wong. Fastercache: Training-free video diffusion model acceleration with high quality. In *The Thirteenth International Conference on Learning Representations*. 3
- [42] Xinyin Ma, Gongfan Fang, and Xinchao Wang. Deepcache: Accelerating diffusion models for free. In *Proceedings of the IEEE/CVF conference on computer vision and pattern recognition*, pages 15762–15772, 2024. 3, 5, 8
- [43] Zehong Ma, Longhui Wei, Feng Wang, Shiliang Zhang, and Qi Tian. Magcache: Fast video generation with magnitude-aware cache. In *The Thirty-ninth Annual Conference on Neural Information Processing Systems*, 2025. 3, 5, 4
- [44] Stephane Mallat. *A wavelet tour of signal processing*. Academic press, 1999. 1
- [45] Chenlin Meng, Robin Rombach, Ruiqi Gao, Diederik Kingma, Stefano Ermon, Jonathan Ho, and Tim Salimans. On distillation of guided diffusion models. In *Proceedings of the IEEE/CVF conference on computer vision and pattern recognition*, pages 14297–14306, 2023. 1
- [46] Henri J Nussbaumer. The fast fourier transform. In *Fast Fourier transform and convolution algorithms*, pages 80–111. Springer, 1981. 5
- [47] Yifan Pu, Zhuofan Xia, Jiayi Guo, Dongchen Han, Qixiu Li, Duo Li, Yuhui Yuan, Ji Li, Yizeng Han, Shiji Song, et al. Efficient diffusion transformer with step-wise dynamic attention mediators. In *European Conference on Computer Vision*, pages 424–441. Springer, 2024. 2
- [48] Robin Rombach, Andreas Blattmann, Dominik Lorenz, Patrick Esser, and Björn Ommer. High-resolution image synthesis with latent diffusion models. In *Proceedings of the IEEE/CVF conference on computer vision and pattern recognition*, pages 10684–10695, 2022. 1, 2
- [49] Chitwan Saharia, William Chan, Saurabh Saxena, Lala Li, Jay Whang, Emily L Denton, Kamyar Ghasemipour, Raphael Gontijo Lopes, Burcu Karagol Ayan, Tim Salimans, et al. Photorealistic text-to-image diffusion models with deep language understanding. *Advances in Neural Information Processing Systems*, 35:36479–36494, 2022. 2, 6

- [50] Tim Salimans and Jonathan Ho. Progressive distillation for fast sampling of diffusion models. In *International Conference on Learning Representations*. 1, 2
- [51] Axel Sauer, Frederic Boesel, Tim Dockhorn, Andreas Blattmann, Patrick Esser, and Robin Rombach. Fast high-resolution image synthesis with latent adversarial diffusion distillation. In *SIGGRAPH Asia 2024 Conference Papers*, pages 1–11, 2024.
- [52] Axel Sauer, Dominik Lorenz, Andreas Blattmann, and Robin Rombach. Adversarial diffusion distillation. In *European Conference on Computer Vision*, pages 87–103. Springer, 2024. 1
- [53] Pratheba Selvaraju, Tianyu Ding, Tianyi Chen, Ilya Zharkov, and Luming Liang. Fora: Fast-forward caching in diffusion transformer acceleration. *arXiv preprint arXiv:2407.01425*, 2024. 3
- [54] Yuzhang Shang, Zhihang Yuan, Bin Xie, Bingzhe Wu, and Yan Yan. Post-training quantization on diffusion models. In *Proceedings of the IEEE/CVF conference on computer vision and pattern recognition*, pages 1972–1981, 2023. 1, 2
- [55] Junhyuk So, Jungwon Lee, Daehyun Ahn, Hyungjun Kim, and Eunhyeok Park. Temporal dynamic quantization for diffusion models. *Advances in neural information processing systems*, 36:48686–48698, 2023. 2, 3
- [56] Jascha Sohl-Dickstein, Eric Weiss, Niru Maheswaranathan, and Surya Ganguli. Deep unsupervised learning using nonequilibrium thermodynamics. In *International conference on machine learning*, pages 2256–2265. pmlr, 2015. 1, 2
- [57] Jiaming Song, Chenlin Meng, and Stefano Ermon. Denoising diffusion implicit models. In *International Conference on Learning Representations*. 2
- [58] Yang Song and Stefano Ermon. Generative modeling by estimating gradients of the data distribution. *Advances in neural information processing systems*, 32, 2019. 1, 2
- [59] Yang Song, Prafulla Dhariwal, Mark Chen, and Ilya Sutskever. Consistency models. In *Proceedings of the 40th International Conference on Machine Learning*, pages 32211–32252, 2023. 2
- [60] Wei Sun, Tao Wang, Xionghuo Min, Fuwang Yi, and Guangtao Zhai. Deep learning based full-reference and no-reference quality assessment models for compressed ugc videos. In *2021 IEEE International Conference on Multimedia & Expo Workshops (ICMEW)*, pages 1–6. IEEE, 2021. 2, 4
- [61] David J Tolhurst, Yoav Tadmor, and Tang Chao. Amplitude spectra of natural images. *Ophthalmic and Physiological Optics*, 12(2):229–232, 1992. 4, 2
- [62] van A Van der Schaaf and JH van van Hateren. Modelling the power spectra of natural images: statistics and information. *Vision research*, 36(17):2759–2770, 1996. 4, 2
- [63] Team Wan, Ang Wang, Baole Ai, Bin Wen, Chaojie Mao, Chen-Wei Xie, Di Chen, Feiwu Yu, Haiming Zhao, Jianxiao Yang, Jianyuan Zeng, Jiayu Wang, Jingfeng Zhang, Jingtong Zhou, Jinkai Wang, Jixuan Chen, Kai Zhu, Kang Zhao, Keyu Yan, Lianghua Huang, Mengyang Feng, Ningyi Zhang, Pandeng Li, Pingyu Wu, Ruihang Chu, Ruili Feng, Shiwei Zhang, Siyang Sun, Tao Fang, Tianxing Wang, Tianyi Gui, Tingyu Weng, Tong Shen, Wei Lin, Wei Wang, Wei Wang, Wenmeng Zhou, Wenten Wang, Wenting Shen, Wenyuan Yu, Xianzhong Shi, Xiaoming Huang, Xin Xu, Yan Kou, Yangyu Lv, Yifei Li, Yijing Liu, Yiming Wang, Yingya Zhang, Yitong Huang, Yong Li, You Wu, Yu Liu, Yulin Pan, Yun Zheng, Yuntao Hong, Yupeng Shi, Yutong Feng, Zeyinzi Jiang, Zhen Han, Zhi-Fan Wu, and Ziyu Liu. Wan: Open and advanced large-scale video generative models. *arXiv preprint arXiv:2503.20314*, 2025. 2, 6, 7
- [64] Zhou Wang, Alan C Bovik, Hamid R Sheikh, and Eero P Simoncelli. Image quality assessment: from error visibility to structural similarity. *IEEE transactions on image processing*, 13(4):600–612, 2004. 6
- [65] Norbert Wiener. *Extrapolation, interpolation, and smoothing of stationary time series*. The MIT press, 1964. 4, 1
- [66] Felix Wimbauer, Bichen Wu, Edgar Schoenfeld, Xiaoliang Dai, Ji Hou, Zijian He, Artsiom Sanakoyeu, Peizhao Zhang, Sam Tsai, Jonas Kohler, et al. Cache me if you can: Accelerating diffusion models through block caching. In *Proceedings of the IEEE/CVF Conference on Computer Vision and Pattern Recognition*, pages 6211–6220, 2024. 3, 5
- [67] Haocheng Xi, Shuo Yang, Yilong Zhao, Chenfeng Xu, Muyang Li, Xiuyu Li, Yujun Lin, Han Cai, Jintao Zhang, Dacheng Li, et al. Sparse video-gen: Accelerating video diffusion transformers with spatial-temporal sparsity. In *Forty-second International Conference on Machine Learning*. 1, 2
- [68] Yifei Xia, Suhan Ling, Fangcheng Fu, Yujie Wang, Huixia Li, Xuefeng Xiao, and Bin Cui. Training-free and adaptive sparse attention for efficient long video generation. *arXiv preprint arXiv:2502.21079*, 2025. 1, 2
- [69] xiaojun ye. calflops: a flops and params calculate tool for neural networks in pytorch framework, 2023. 6
- [70] Chenglin Yang, Celong Liu, Xueqing Deng, Dongwon Kim, Xing Mei, Xiaohui Shen, and Liang-Chieh Chen. 1.58-bit flux. *arXiv preprint arXiv:2412.18653*, 2024. 1
- [71] Shuo Yang, Haocheng Xi, Yilong Zhao, Muyang Li, Jintao Zhang, Han Cai, Yujun Lin, Xiuyu Li, Chenfeng Xu, Kelly Peng, et al. Sparse videogen2: Accelerate video generation with sparse attention via semantic-aware permutation. *arXiv preprint arXiv:2505.18875*, 2025. 1, 2
- [72] Xingyi Yang, Daquan Zhou, Jiashi Feng, and Xinchao Wang. Diffusion probabilistic model made slim. In *Proceedings of the IEEE/CVF Conference on computer vision and pattern recognition*, pages 22552–22562, 2023. 4, 1
- [73] Cuihong Yu, Cheng Han, and Chao Zhang. Dmfft: improving the generation quality of diffusion models using fast fourier transform. *Scientific Reports*, 15(1):10200, 2025. 1
- [74] Zhihang Yuan, Hanling Zhang, Lu Pu, Xuefei Ning, Linfeng Zhang, Tianchen Zhao, Shengen Yan, Guohao Dai, and Yu Wang. Ditfastattn: Attention compression for diffusion transformer models. *Advances in Neural Information Processing Systems*, 37:1196–1219, 2024. 1, 2
- [75] Evelyn Zhang, Jiayi Tang, Xuefei Ning, and Linfeng Zhang. Training-free and hardware-friendly acceleration for diffusion models via similarity-based token pruning. In *Proceed-*

- ings of the AAAI Conference on Artificial Intelligence*, pages 9878–9886, 2025. [1](#), [2](#), [3](#), [4](#)
- [76] Jintao Zhang, Pengle Zhang, Jun Zhu, Jianfei Chen, et al. Sageattention: Accurate 8-bit attention for plug-and-play inference acceleration. In *The Thirteenth International Conference on Learning Representations*. [1](#)
- [77] Richard Zhang, Phillip Isola, Alexei A Efros, Eli Shechtman, and Oliver Wang. The unreasonable effectiveness of deep features as a perceptual metric. In *Proceedings of the IEEE conference on computer vision and pattern recognition*, pages 586–595, 2018. [6](#)
- [78] Wenliang Zhao, Lujia Bai, Yongming Rao, Jie Zhou, and Jiwen Lu. Unipc: A unified predictor-corrector framework for fast sampling of diffusion models. *Advances in Neural Information Processing Systems*, 36:49842–49869, 2023. [2](#)
- [79] Xuanlei Zhao, Xiaolong Jin, Kai Wang, and Yang You. Real-time video generation with pyramid attention broadcast. In *The Thirteenth International Conference on Learning Representations*. [1](#), [3](#)
- [80] Chang Zou, Xuyang Liu, Ting Liu, Siteng Huang, and Linfeng Zhang. Accelerating diffusion transformers with token-wise feature caching. In *The Thirteenth International Conference on Learning Representations*, . [6](#)
- [81] Zhen Zou, Jie Huang, Hu Yu, and Feng Zhao. Feb-cache: Frequency-guided exposure bias reduction for enhancing diffusion transformer caching. Available at SSRN 5584552, . [3](#)

SeaCache: Spectral-Evolution-Aware Cache for Accelerating Diffusion Models

Supplementary Material

We first present the derivation analysis of the linear diffusion process. We then provide additional experiments that further validate the effectiveness of the proposed SeaCache.

7. Derivation of Optimal Linear Response

To design a filter that reflects spectral evolution, we formalize how the effective frequency band changes across timesteps. Motivated by Spectral Diffusion [72] and Wiener Filtering [65], we adopt the timestep-dependent frequency response derived from the optimal linear denoiser h_t^* .¹

Setup and assumptions. We consider the linear mixture of iterative denoising generative models (DPMs and RFs) at timestep t ,

$$x_t = a_t x_0 + b_t \epsilon, \quad \epsilon \sim \mathcal{N}(0, \mathbf{I}), \quad (9)$$

where x_0 is the clean signal, assumed to be wide-sense stationary, and ϵ is zero-mean white Gaussian noise with flat power spectral density $S_\epsilon(f) = 1$. We also assume that x_0 and ϵ are independent.

The Fourier-domain version of Eq. (9) is

$$\mathcal{X}_t(f) = a_t \mathcal{X}_0(f) + b_t \mathcal{E}(f), \quad (10)$$

where $\mathcal{X}_0(f)$, $\mathcal{X}_t(f)$, and $\mathcal{E}(f)$ are the Fourier transforms of x_0 , x_t and ϵ at frequency f , respectively.

The filter h_t estimates x_0 from x_t as

$$\hat{x}_0 = h_t * x_t \iff \hat{\mathcal{X}}_0(f) = \mathcal{H}_t(f) \mathcal{X}_t(f), \quad (11)$$

where h_t is a linear reconstruction estimator, $\mathcal{H}_t(f)$ is the frequency response of h_t , and \hat{x}_0 , $\hat{\mathcal{X}}_0(f)$ are the estimated signal and its Fourier counterpart, respectively.

We define the signal reconstruction MSE objective, which is equivalent to the denoising objective of diffusion models,

$$J_t = \|h_t * x_t - x_0\|_2^2, \quad h_t^* = \arg \min_{h_t} \mathbb{E}[J_t], \quad (12)$$

where the expectation is taken over (x_0, ϵ) .

Frequency-domain MSE expansion. By Parseval's theorem [44], the reconstruction MSE (Eq. (12)) decomposes

¹Throughout this section, “*” denotes convolution in the frequency domain, the superscript “*” denotes the optimal solution, and (\cdot) denotes complex conjugation of Fourier coefficients.

as an integral over frequencies. Since $\mathcal{H}_t(f)$ acts independently at each frequency, minimizing the total MSE is equivalent to minimizing $J_t(f)$ for every f ,

$$J_t(f) = \mathbb{E} \left[\left| \mathcal{H}_t(f) \mathcal{X}_t(f) - \mathcal{X}_0(f) \right|^2 \right]. \quad (13)$$

We now expand $J_t(f)$ using standard complex-valued quadratic expansion:

$$\begin{aligned} J_t(f) &= \mathbb{E} \left[\left| \mathcal{H}_t(f) \mathcal{X}_t(f) - \mathcal{X}_0(f) \right|^2 \right] \\ &= \mathbb{E} \left[(\mathcal{H}_t(f) \mathcal{X}_t(f) - \mathcal{X}_0(f)) (\overline{\mathcal{H}_t(f) \mathcal{X}_t(f) - \mathcal{X}_0(f)}) \right] \\ &= |\mathcal{H}_t(f)|^2 \mathbb{E} [|\mathcal{X}_t(f)|^2] - \mathcal{H}_t(f) \mathbb{E} [\mathcal{X}_t(f) \overline{\mathcal{X}_0(f)}] \\ &\quad - \overline{\mathcal{H}_t(f)} \mathbb{E} [\mathcal{X}_0(f) \overline{\mathcal{X}_t(f)}] + \mathbb{E} [|\mathcal{X}_0(f)|^2], \end{aligned} \quad (14)$$

where all quantities are evaluated at frequency f .

We next simplify the two expectation terms $\mathbb{E}[\mathcal{X}_0(f) \overline{\mathcal{X}_t(f)}]$ and $\mathbb{E}[|\mathcal{X}_t(f)|^2]$, which will be used in the subsequent derivation. Let $S_x(f)$ denote the power spectrum of x_0 . The first term can be written as

$$\begin{aligned} \mathbb{E}[\mathcal{X}_0(f) \overline{\mathcal{X}_t(f)}] &= \mathbb{E}[\mathcal{X}_0(f) (a_t \overline{\mathcal{X}_0(f)} + b_t \overline{\mathcal{E}(f)})] \\ &= a_t \mathbb{E}[|\mathcal{X}_0(f)|^2] + b_t \mathbb{E}[\mathcal{X}_0(f) \overline{\mathcal{E}(f)}] \\ &= a_t \mathbb{E}[|\mathcal{X}_0(f)|^2] \\ &= a_t S_x(f), \end{aligned} \quad (15)$$

since we assume that x_0 is wide-sense stationary and independent of the noise ϵ , so $\mathbb{E}[\mathcal{X}_0(f) \overline{\mathcal{E}(f)}] = 0$ in Eq. (15). Next, we expand the second expectation term:

$$\begin{aligned} \mathbb{E}[|\mathcal{X}_t(f)|^2] &= \mathbb{E}[(a_t \mathcal{X}_0(f) + b_t \mathcal{E}(f)) (a_t \overline{\mathcal{X}_0(f)} + b_t \overline{\mathcal{E}(f)})] \\ &= a_t^2 \mathbb{E}[|\mathcal{X}_0(f)|^2] + b_t^2 \mathbb{E}[|\mathcal{E}(f)|^2] \\ &\quad + a_t b_t \mathbb{E}[\mathcal{X}_0(f) \overline{\mathcal{E}(f)}] + a_t b_t \mathbb{E}[\overline{\mathcal{X}_0(f)} \mathcal{E}(f)] \\ &= a_t^2 \mathbb{E}[|\mathcal{X}_0(f)|^2] + b_t^2 \mathbb{E}[|\mathcal{E}(f)|^2] \\ &= a_t^2 S_x(f) + b_t^2 S_\epsilon(f) \\ &= a_t^2 S_x(f) + b_t^2, \end{aligned} \quad (16)$$

since in Eq. (16), the cross terms vanish because of independence, $\mathbb{E}[\mathcal{X}_0(f) \mathcal{E}(f)] = \mathbb{E}[\overline{\mathcal{X}_0(f)} \overline{\mathcal{E}(f)}] = 0$, and whiteness of the noise ϵ implies $\mathbb{E}[|\mathcal{E}(f)|^2] = S_\epsilon(f) = 1$.

Optimality by differentiation. Differentiating Eq. (14) with respect to $\overline{\mathcal{H}_t(f)}$ using Wirtinger derivative [5] and setting the result to zero to find the optimal linear filter under the linear MMSE criterion, we obtain

$$\frac{\partial J_t(f)}{\partial \overline{\mathcal{H}_t(f)}} = \mathcal{H}_t(f) \mathbb{E}[|\mathcal{X}_t(f)|^2] - \mathbb{E}[\mathcal{X}_0(f) \overline{\mathcal{X}_t(f)}] = 0. \quad (17)$$

Table 5. Runtime overhead of SEA filtering per sample, averaged over 10 runs.

Model	SEA Filter (s)	Latency (s)	Overhead (%)
FLUX (2D FFT)	0.058	9.4	0.6
HunyuanVideo (3D FFT)	0.362	90.8	0.4

Table 6. Runtime overhead of SEA filtering per sample on Wan2.1-14B-T2V at different output resolutions.

Resolution	SEA Filter (s)	Total Latency (s)	Overhead (%)
480p	0.668	161.5	0.41
720p	1.539	561.1	0.27

Using Eqs. (15) and (16), the unique minimizer is

$$\mathcal{H}_t^*(f) = \frac{\mathbb{E}[\mathcal{X}_0(f)\overline{\mathcal{X}_t(f)}]}{\mathbb{E}[|\mathcal{X}_t(f)|^2]} = \frac{a_t S_x(f)}{a_t^2 S_x(f) + b_t^2}, \quad (18)$$

where $\mathcal{H}_t^*(f)$ is the Fourier transform of h_t^* . We define the optimal frequency response

$$G_t(f) \triangleq \mathcal{H}_t^*(f). \quad (19)$$

Power-law prior. We adopt an empirical natural-image power-law assumption for the power spectrum [7, 18, 61, 62],

$$S_x(f) \simeq A |f|^{-\beta}, \quad (20)$$

where $A > 0$ is an amplitude scaling factor and β is a frequency exponent. In our experiments, we set $A = 1$ and $\beta = 2$ for images and $\beta = 3$ for videos. Substituting this prior into the optimal response in Eq. (18) gives

$$G_t(f) = \frac{a_t |f|^{-\beta}}{a_t^2 |f|^{-\beta} + b_t^2}, \quad (21)$$

which shows that the effective passband widens as a_t increases (*spectral evolution*). Note that the SEA filter used in our method $G_t^{\text{norm}}(f)$ is a normalized variant of $G_t(f)$. Its form is provided in the main manuscript.

8. Runtime Overhead of SEA Filtering

At every sampling step, SeaCache inserts an additional FFT \rightarrow frequency-domain filtering \rightarrow iFFT pass to construct SEA-filtered features. Thus, we measure how much of the end-to-end sampling time this pass occupies under a 50% caching ratio, keeping all other settings identical to the main experiments. For *FLUX* [28, 29] with SeaCache, the SEA filtering pass takes on average 0.058 s per sample out of a total latency of 9.4 s, corresponding to only about 0.6% of the overall generation time. For *HunyuanVideo* [27] with SeaCache, the 3D FFT-based SEA filtering costs 0.362 s per sample while the total latency is 90.8 s, roughly 0.4% of the end-to-end runtime. As summarized in Tab. 5, the SEA filtering introduces a negligible runtime overhead while enabling substantially better preservation of the original outputs compared to prior caching schemes.

To further quantify the SEA filter and FFT/iFFT overhead on a large text-to-video (T2V) diffusion model, we additionally profile *LightX2V* [11] on Wan2.1-14B-T2V [63] under a 50% caching ratio, using a single Blackwell Pro 6000 GPU, while keeping all other settings identical. Since sampling is performed in a compressed latent space, the SEA filtering pass occupies only a tiny fraction of the end-to-end runtime. As shown in Tab. 6, the overhead stays below 1% in practice and remains small even when increasing the output resolution (0.41% at 480p and 0.27% at 720p).

9. Compatibility with Fast Inference Works

We additionally validate SeaCache on Wan2.1-T2V under two orthogonal acceleration settings: (i) a distilled sampler (*LightX2V* [11], 16-step) and (ii) an efficient-attention variant (*Jenga* [75], 50-step), using each method’s default configuration. All results are evaluated on *VBench* [23] at 480p with 41 frames, using videos generated from 50 randomly sampled *VBench* prompts. Under comparable refresh ratio budgets, SeaCache consistently improves quality over TeaCache and vanilla step reduction, as shown in Tab. 12.

10. Additional Evaluation

10.1. Quantitative Comparison in T2V Generation

VBench on *HunyuanVideo*. We evaluate SeaCache against TeaCache [33] and TaylorSeer [19] on all *VBench* [23] dimensions (Tab. 7), where the upper rows correspond to the 50% refresh-ratio budget and the lower rows to the 30% budget. All detailed settings follow the main manuscript. Aggregating by average rank across dimensions (Tab. 9), SeaCache ranks first under both budgets, scoring 1.91 vs. 2.03/2.06 at $\approx 50\%$, and 1.75 vs. 2.16/2.09 at $\approx 30\%$. This indicates the strongest overall performance across *VBench* dimensions on *HunyuanVideo*.

VBench on *Wan2.1 1.3B*. We repeat the evaluation on all *VBench* dimensions for *Wan2.1* [63] (Tab. 8) with the same two budgets and the same experimental details as in the main manuscript. In aggregate (Tab. 10), SeaCache delivers stable performance across dimensions, ranking second under both budgets, 1.97 at $\approx 50\%$ (vs. the best 1.91) and 2.13 at $\approx 30\%$ (vs. the best 1.53). Although our cache configurations are designed to closely track the original full-refresh sampling trajectory, the *VBench* results on *Wan2.1* still show that SeaCache provides robust performance across dimensions and refresh-ratio budgets.

CompressedVQA on T2V. To further quantify how caching affects video quality, we report scores from *CompressedVQA* [60], a full-reference video quality assessment (VQA) metric. For each video, we treat the uncached trajectory as the reference and compute single-scale and multi-scale scores between the cached outputs. Tab. 11 summa-

Table 7. VBench metrics in *HunyuanVideo*.

Models	Subject Consistency	Background Consistency	Temporal Flickering	Motion Smoothness	Dynamic Degree	Aesthetic Quality	Imaging Quality	Object Class
TeaCache ($\delta=0.12$)	95.59%	95.99%	99.14%	98.77%	62.50%	60.92%	62.07%	86.31%
TaylorSeer ($S=2$)	95.75%	96.20%	99.09%	98.83%	63.89%	60.93%	62.73%	83.47%
SeaCache ($\delta=0.19$)	95.77%	96.28%	99.15%	98.88%	62.50%	60.55%	62.01%	85.28%
TeaCache ($\delta=0.2$)	95.57%	96.04%	99.18%	98.76%	62.50%	60.28%	60.28%	86.47%
TaylorSeer ($S=3$)	95.67%	96.18%	99.07%	98.86%	63.89%	60.64%	63.25%	82.20%
SeaCache ($\delta=0.35$)	95.78%	96.35%	99.20%	98.92%	61.11%	60.00%	61.02%	82.59%

Models	Multiple Objects	Human Action	Color	Spatial Relationship	Scene	Temporal Style	Appearance Style	Overall Consistency
TeaCache ($\delta=0.12$)	64.71%	96.00%	89.61%	61.84%	42.81%	24.39%	19.85%	26.91%
TaylorSeer ($S=2$)	58.38%	95.00%	90.87%	60.80%	40.48%	24.44%	19.89%	26.60%
SeaCache ($\delta=0.19$)	63.64%	94.00%	90.26%	62.96%	40.92%	24.66%	19.83%	26.63%
TeaCache ($\delta=0.2$)	63.34%	92.00%	89.81%	59.65%	44.48%	24.26%	19.93%	26.68%
TaylorSeer ($S=3$)	60.06%	92.00%	89.26%	57.78%	41.72%	24.35%	20.02%	26.57%
SeaCache ($\delta=0.35$)	58.38%	94.00%	92.24%	60.63%	42.88%	24.34%	20.10%	26.33%

Table 8. VBench metrics in *Wan2.1 I.3B*.

Models	Subject Consistency	Background Consistency	Temporal Flickering	Motion Smoothness	Dynamic Degree	Aesthetic Quality	Imaging Quality	Object Class
TeaCache ($\delta=0.09$)	95.89%	97.09%	98.30%	97.37%	81.94%	62.48%	67.88%	80.46%
TaylorSeer ($S=2$)	95.78%	96.90%	98.37%	97.47%	88.89%	62.14%	68.08%	82.75%
SeaCache ($\delta=0.2$)	95.96%	97.05%	98.20%	97.41%	84.72%	62.31%	68.01%	81.17%
TeaCache ($\delta=0.15$)	96.04%	97.02%	98.21%	97.35%	83.33%	62.25%	67.47%	80.22%
TaylorSeer ($S=3$)	95.32%	96.54%	98.21%	97.48%	84.72%	60.85%	67.83%	78.32%
SeaCache ($\delta=0.35$)	96.03%	97.00%	98.12%	97.39%	81.94%	61.71%	67.66%	79.75%

Models	Multiple Objects	Human Action	Color	Spatial Relationship	Scene	Temporal Style	Appearance Style	Overall Consistency
TeaCache ($\delta=0.09$)	52.67%	72.00%	92.95%	71.46%	23.91%	23.07%	20.06%	23.42%
TaylorSeer ($S=2$)	53.73%	70.00%	91.22%	75.48%	30.09%	22.75%	20.13%	23.41%
SeaCache ($\delta=0.2$)	53.89%	70.00%	93.01%	69.50%	22.89%	23.32%	20.04%	23.51%
TeaCache ($\delta=0.15$)	51.91%	72.00%	90.56%	67.67%	24.27%	22.98%	20.09%	23.58%
TaylorSeer ($S=3$)	45.05%	69.00%	87.83%	60.79%	20.20%	22.37%	20.64%	23.17%
SeaCache ($\delta=0.35$)	53.20%	68.00%	89.67%	69.57%	23.62%	22.96%	20.06%	23.18%

Table 9. Comparison of avg. rank on VBench in *HunyuanVideo*.

Method ($\approx 50\%$)	Rank \downarrow	Method ($\approx 30\%$)	Rank \downarrow
TeaCache ($\delta=0.12$)	2.03	TeaCache ($\delta=0.20$)	2.16
TaylorSeer ($S=2$)	2.06	TaylorSeer ($S=3$)	2.09
SeaCache ($\delta=0.19$)	1.91	SeaCache ($\delta=0.35$)	1.75

Table 10. Comparison of avg. rank on VBench in *Wan2.1 I.3B*.

Method ($\approx 50\%$)	Rank \downarrow	Method ($\approx 30\%$)	Rank \downarrow
TeaCache ($\delta=0.09$)	2.13	TeaCache ($\delta=0.15$)	1.53
TaylorSeer ($S=2$)	1.91	TaylorSeer ($S=3$)	2.34
SeaCache ($\delta=0.30$)	1.97	SeaCache ($\delta=0.35$)	2.13

Table 11. CompressedVQA [60] scores on *HunyuanVideo* and *Wan2.1 1.3B* under single-scale and multi-scale settings.

<i>HunyuanVideo</i>			<i>Wan2.1 1.3B</i>		
Method ($\approx 50\%$)	Single-scale score \uparrow	Multi-scale score \uparrow	Method ($\approx 50\%$)	Single-scale score \uparrow	Multi-scale score \uparrow
TeaCache ($\delta=0.12$)	2.72	2.76	TeaCache ($\delta=0.09$)	2.97	3.03
TaylorSeer ($S=2$)	2.92	2.95	TaylorSeer ($S=2$)	1.90	1.95
SeaCache ($\delta=0.19$)	3.98	3.99	SeaCache ($\delta=0.30$)	3.93	3.95
Method ($\approx 30\%$)	Single-scale score \uparrow	Multi-scale score \uparrow	Method ($\approx 30\%$)	Single-scale score \uparrow	Multi-scale score \uparrow
TeaCache ($\delta=0.20$)	2.11	2.16	TeaCache ($\delta=0.15$)	2.44	2.49
TaylorSeer ($S=3$)	2.22	2.26	TaylorSeer ($S=3$)	1.38	1.42
SeaCache ($\delta=0.35$)	3.13	3.17	SeaCache ($\delta=0.35$)	3.09	3.11

Table 12. Compatibility with fast inference works on *Wan2.1-T2V*: *LightX2V* [11] (14B, 16-step) and *Jenga* [75] (1.3B, 50-step), evaluated under comparable refresh ratio budgets.

	Method	Refresh Ratio	PSNR	LPIPS	SSIM
Distillation (<i>LightX2V</i> [11])	Vanilla	25% (4 steps)	11.444	0.475	0.405
	TeaCache	25% (4 steps)	11.762	0.480	0.420
	SeaCache	25% (4 steps)	11.926	0.465	0.432
Efficient Attn. (<i>Jenga</i> [75])	Vanilla	50% (25 steps)	15.154	0.357	0.604
	TeaCache	50% (25 steps)	19.463	0.191	0.744
	SeaCache	48% (24 steps)	24.453	0.097	0.852
	Vanilla	32% (16 steps)	13.440	0.455	0.534
	TeaCache	32% (16 steps)	17.692	0.259	0.681
	SeaCache	32% (16 steps)	20.259	0.194	0.748

rizes the results on *HunyuanVideo* and *Wan2.1 1.3B* at two cache budgets with refresh ratios of approximately 50% and 30%. Across both models and budgets, SeaCache consistently achieves the highest single-scale and multi-scale scores among all caching baselines, indicating that it best preserves the visual quality of the original trajectory while still enjoying substantial reductions in the refresh ratio.

10.2. Comparison with MagCache

We further compare SeaCache with MagCache [43] under matched refresh ratios by tuning the cache threshold δ . We use the default MagCache configuration and report results. For *FLUX.1-dev*, we follow the manuscript protocol (DrawBench, 200 prompts). For *Wan2.1 1.3B T2V*, we evaluate at 480p with 41 frames using 50 randomly sampled prompts from VBench [23]. As shown in Tab. 13, SeaCache consistently improves quality at the same refresh ratio. We attribute this to SeaCache’s input-adaptive redundancy estimation, whereas MagCache relies on a fixed magnitude threshold, which is less responsive to content- and timestep-dependent variations.

10.3. Qualitative Comparison in T2I Generation

In Fig. 12, we provide additional qualitative comparisons on *FLUX* at refresh ratios of approximately 50% (top panel) and 30% (middle panel), along with an additional set of ex-

amples at both cache budgets in the bottom panel.

At 50% refresh ratio in the top-left of Fig 12, SeaCache preserves a clean water surface without the blocky artifacts or texture distortions that appear in the baselines. In the top-right example, the baselines either generate a blurry lemon or fail to capture the fluid dynamics inside the bottle, whereas SeaCache correctly synthesizes both the glass bottle and the orange liquid, closely matching the full-compute original reference.

At a more aggressive 30% refresh ratio in the middle panel, SeaCache again stays closest to the full-compute reference. In the middle-left example, only SeaCache reconstructs seven well-formed stars consistent with the original, while competing methods either miss or severely deform several stars. In the middle-right example, SeaCache produces five chopsticks with consistent length and color, whereas the baselines generate chopsticks with mismatched geometry and appearance.

In the bottom panel of Fig. 12, we further compare the same text prompts across different cache budgets using the same seed. In the top row of the panel, for the prompt requesting exactly the word “CUBE,” the baselines repeatedly hallucinate cube-like patterns in the background, whereas SeaCache is the only method that successfully renders the intended text. In the last row of the panel, all methods generate six wooden ice creams, but the baselines produce slightly different designs or colors compared to the full-compute reference, while SeaCache most closely matches the original design.

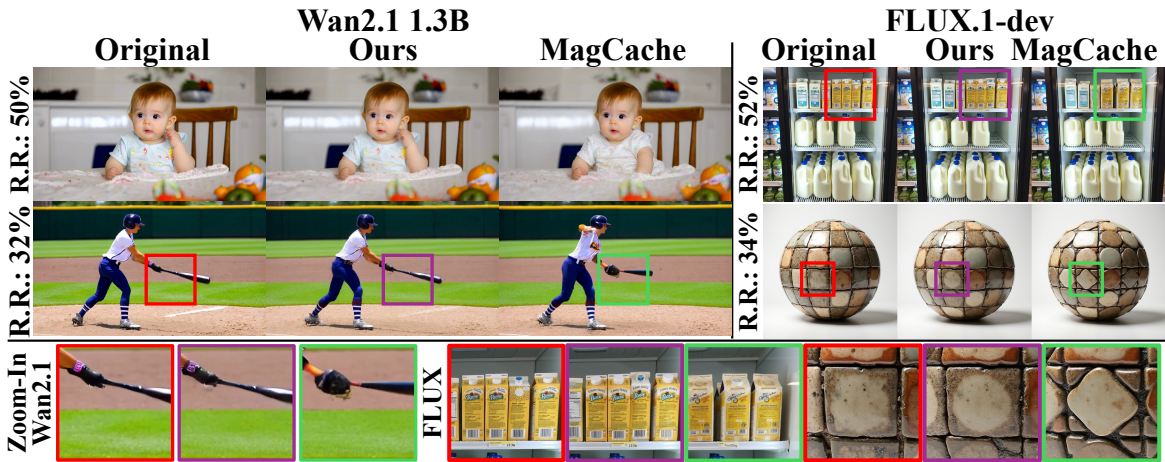
These additional cases further support that SeaCache best preserves the original content and layout while operating under the same cache budgets.

10.4. Qualitative Comparison in T2V Generation

Fig. 13 presents further qualitative comparisons on *HunyuanVideo* and *Wan2.1 1.3B*, respectively. For each prompt, we horizontally concatenate the same intermediate frame index from the full-compute reference and all caching variants to isolate per-frame differences. On *HunyuanVideo* at

Table 13. Comparison with MagCache at matched refresh ratios (R.R.) by tuning the cache threshold δ . We report full-reference quality against the uncached outputs on *FLUX.1-dev* and *Wan2.1 1.3B-T2V*. SeaCache shows higher PSNR and lower LPIPS than MagCache [43] at the same refresh ratio.

Method	R.R.	PSNR \uparrow	LPIPS \downarrow	Method	R.R.	PSNR \uparrow	LPIPS \downarrow
<i>FLUX.1-dev</i> (50-step)							
MagCache ($\delta=0.04$) [43]	52%	29.96	0.056	MagCache ($\delta=0.15$) [43]	34%	24.73	0.126
SeaCache ($\delta=0.215$)	52%	30.37	0.053	SeaCache ($\delta=0.4$)	34%	24.97	0.123
MagCache ($\delta=0.07$) [43]	44%	27.89	0.079	MagCache ($\delta=0.35$) [43]	28%	22.51	0.179
SeaCache ($\delta=0.27$)	44%	28.09	0.072	SeaCache ($\delta=0.55$)	28%	23.01	0.172
<i>Wan2.1 1.3B T2V</i> (50-step)							
MagCache ($\delta=0.055$) [43]	50%	25.55	0.079	MagCache ($\delta=0.15$) [43]	32%	19.32	0.226
SeaCache ($\delta=0.19$)	49%	29.55	0.047	SeaCache ($\delta=0.4$)	32%	21.98	0.156



Wan (50%): “A person is baby waking up”, **Wan (32%):** “A baseball bat”,
FLUX (52%): “A grocery store refrigerator has pint cartons of milk on the top shelf,
quart cartons on the middle shelf, and gallon plastic jugs on the bottom shelf”,
FLUX (34%): “A cube made of denim. A cube with the texture of denim”

Figure 11. Qualitative comparison between MagCache and SeaCache at matched refresh ratios on *FLUX.1-dev* and *Wan2.1 1.3B T2V*. At the same refresh ratio, SeaCache better preserves the uncached trajectory while reducing refresh operations.

a 30% refresh ratio, the baselines exhibit severe artifacts around the hands during the Taichi motion, while SeaCache preserves a plausible pose with smooth limb contours. At 50% refresh, the baselines render a skateboard that appears to float above the surfboard, whereas SeaCache correctly places the skateboard in contact with the surfboard, matching the original video, as shown in the right side of Fig. 13.

On *Wan2.1 1.3B* at a 30% refresh ratio the baselines introduce noticeable distortions near the truck wheels and bicycles, but these artifacts do not appear in the SeaCache outputs, as visualized in Fig. 13. At 50% refresh, competing methods either cause food items on the table to disappear or introduce artifacts on the panda, while SeaCache closely follows the full-compute trajectory without these failures. Overall, these qualitative results indicate that SeaCache better tracks the original dynamics and adheres more faithfully

to the text prompts while avoiding objectionable artifacts.

11. Limitation

To derive the optimal linear filter, we adopt several simplifying assumptions that make the spectral response analytically tractable, even though they need not hold exactly in practice. We model the signal spectrum with a power law under a radial view, whereas generated samples, particularly at later timesteps or in highly synthetic backgrounds with no salient objects, can deviate from this behavior. We also assume wide-sense stationarity and independence between signal and noise. When these conditions are violated, the closed-form linear filter is no longer strictly optimal and can introduce bias.

In addition, our analysis is formulated in the image or

video domain, while most modern generative models operate in a learned latent space. The encoder can reshape the spectrum, so the latent distribution may differ from the assumed pixel-domain power-law model, and our filter then only approximates the optimal latent-space response.

A promising extension is to relax these assumptions by estimating per-timestep spectra, designing content-aware filters directly in the latent space, and augmenting them with lightweight nonlinear corrections, while preserving the plug-and-play nature of our cache policy. These extensions would reduce the gap between the assumed and actual signal models and further improve fidelity under real-world deviations from our assumptions.

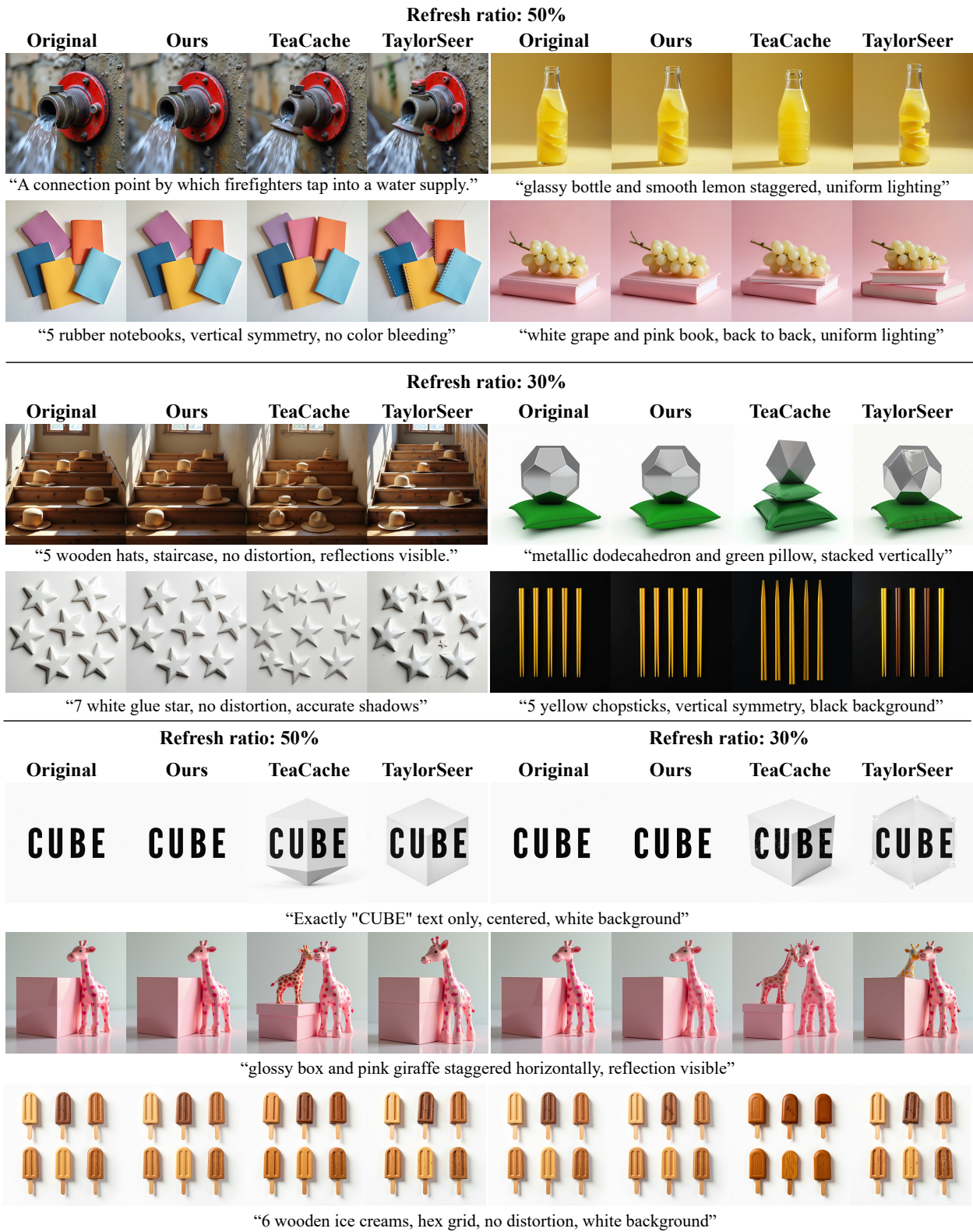
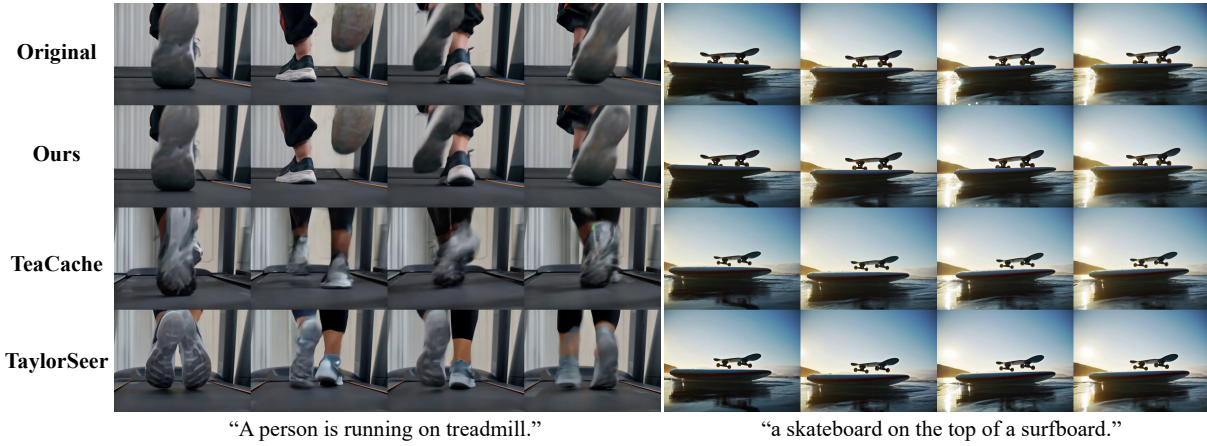
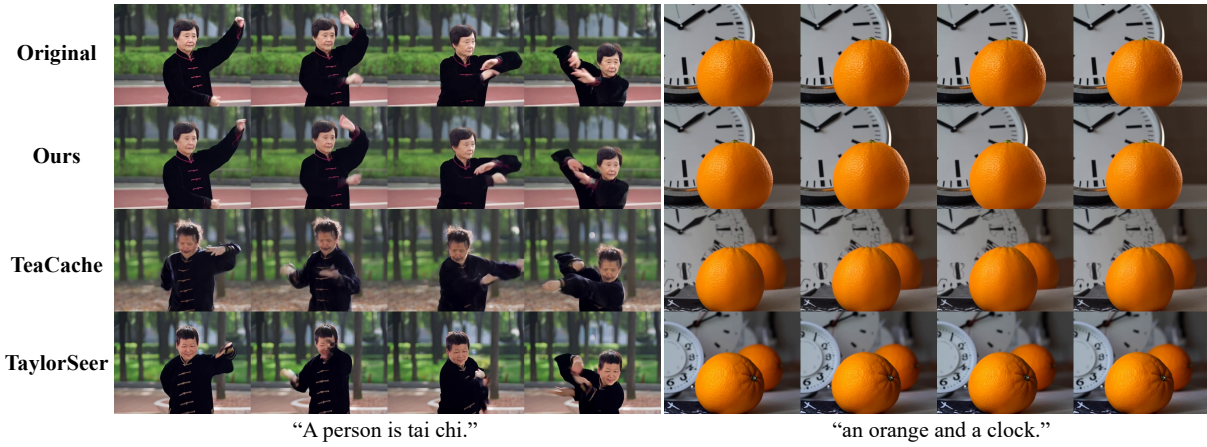


Figure 12. Additional qualitative comparison of SeaCache and baselines on *FLUX* at refresh ratios of approximately 30% and 50%.

HunyuanVideo, Refresh ratio: 50%



HunyuanVideo, Refresh ratio: 30%



Wan2.1 1.3B, Refresh ratio: 50%



Wan2.1 1.3B, Refresh ratio: 30%



Figure 13. Additional T2V qualitative comparison of SeaCache and baselines at refresh ratios of approximately 30% and 50%.